Dual-porosity model of liquid extraction by pressing from biological tissue modified by electroporation

Samo Mahnič-Kalamiza [a,b,*], Eugène Vorobiev [a]

[a] University of Technology of Compiègne, Centre de Recherches de Royallieu – BP 20529, 60205 Compiègne Cedex, France
[b] University of Ljubljana, Faculty of Electrical Engineering, Tržaška c. 25, SI-1000 Ljubljana, Slovenia

ABSTRACT

The objective of this study is to provide insight into the phenomena related with juice expression from electroporated tissue. We propose an analytical model and study consolidation behaviour of a block of tissue during pressing; before and after electroporation. By the dual-porosity approach, we treat compressibility and hydraulic permeability of intracellular and extracellular space separately. Initial parameter estimations are based on previously published studies (for hydraulic permeability), or analysis of modelled data (for compressibility moduli). Good agreement between simulations and experiments performed is then obtained by optimization (i.e. fitting). Impact of electroporation on membrane permeability is theoretically estimated and elucidated via the extraction–consolidation model; results are compared with experimental kinetics for validation and evaluation of model performance. Permeability coefficient estimates from literature proved valuable as initial approximations, and the model results were able to fit experimental data with high accuracy, clearly demonstrating the power of the proposed approach.

© 2014 Elsevier Ltd. All rights reserved.

1. Introduction

Pressing is an important industrial operation for extraction of valuable liquid from a solid–liquid mixture that constitutes biological tissue (Schwartzberg, 1997), or tissue dewatering if the objective is material dehydration (Aguilera et al., 2003). To aid in the understanding of the governing processes, the solid–liquid expression (i.e. extraction by pressing) from vegetable tissues has been studied and modelled (Lanoiselle et al., 1996; Schwartzberg, 1997).

Intact biological tissue exhibits considerable resistance to pressure, i.e. low compressibility and permeability (Buttersack and Basler, 1991). To alleviate this problem, a range of treatments exists in order to enhance and economise juice extraction and tissue dehydration. By nature, these treatments are mechanical, chemical (Binkley and Wiley, 1981), enzymatic (Shankar et al., 1997), thermal (Poel et al., 1998; Praporscic et al., 2006), or electrical (Bazhal and Vorobiev, 2000; Knorr et al., 1994; Luengo et al., 2013; Sack et al., 2008; Vorobiev and Lebovka, 2010; Wiktor and Witrowa-Rajchert, 2012). Application of one or of a combination of several of these treatments damages cellular material, thus increasing its permeability. The treatments can be applied before or during pressing (Bazhal et al., 2001), however, simultaneous application often demands modifications of the existing industrial setup and therefore these operations are most interesting as pre-treatments, applied before the pressing stage.

The permeability of cells in intact plant tissue is at least five orders of magnitude lower than permeability of the extracellular matrix (Buttersack and Basler, 1991). Therefore, the primary objective of pre-treatment is the permeabilization of the cellular membrane. However, different treatments influence the tissue structure differently. The resulting yield and quality of extract or degree of dehydration do not depend only on the specific amount of energy delivered to the material. They are also functions of the chosen treatment and the protocol of treatment application. For example, mechanical treatment (e.g. slicing, grinding) or thermal treatment damage not only cell membranes, but also cell walls (Poel et al., 1998; Llano et al., 2003; Vicente et al., 2005). On the other hand, electrical treatment such as electroporation (also known as pulsed electric field treatment or PEF) can leave the extracellular structures largely intact (Bouzrara and Vorobiev, 2003; Fincan and Dejmek, 2002). While electroporation seems to have no profound effect on cell walls, it is inducing cell permeabilization to a varying degree, or even leading to complete destruction of cellular

* Corresponding author at: Université de Technologie de Compiègne (UTC), Département de Génie des Procédés Industriels, Laboratoire Transformations Intégrées de la Matière Renouvelable, Centre de Recherches de Royallieu – BP 20529, 60205 Compiègne Cedex, France. Tel.: +33 6 52 17 30 92.
   E-mail addresses: samo.mahnic@utc.fr, samo.mahnic-kalamiza@fe.uni-lj.si, samo.mahnic@gmail.com (S. Mahnič-Kalamiza).

Nomenclature

A	cell average surface (also pore surface, membrane surface – see subscripts) (m^2)
e	void ratio (liquid to solid volume) (−)
G_e, G_i	compressibility moduli of extra/intracellular space as defined through void ratio e (Pa)
$G_{\varepsilon,e}$, $G_{\varepsilon,i}$	compressibility moduli of extra/intracellular space as defined through porosity ε (Pa)
f_p	average pore surface fraction per cell (−)
h	tissue sample thickness (m)
k	intrinsic hydraulic permeability (m^2)
L_p	hydraulic permeability as measured by experiments (m MPa^{-1} s^{-1})
l	length of the fluid conduit (membrane thickness, pore length, tissue sample thickness in L_p measurements) (m)
m, n	summation indices (−)
P_E	externally applied pressure (via piston) (Pa)
p_e, p_i	liquid pressure in extra/intracellular space (Pa)
$p_{e,S}$, $p_{i,S}$	solid pressure in extra/intracellular space (Pa)
q	liquid flux (flow per area) velocity (m s^{-1})
Q	liquid flow velocity (m^3 s^{-1})
R	spherical cell radius (without membrane) (m)
r	integration variable
r_p	pore radius (m)
S	tissue sample deformation (m)
s	relative (normalized) deformation (−)
t	model/experiment time (s)

V	average cell volume (m^3)
V_m	membrane volume (m^3)
z	spatial coordinate

Subscripts

c	cell
e	extracellular space (medium)
i	intracellular space (medium)
m	membrane
p	pore (except in L_p)
S	solid
∞	infinity

Greek letters

α	proportionality coefficient in v_{i-e} (−)
Δ	finite difference (in e.g. pressure drop)
δ	short-hand for $1 + G_{\varepsilon,e}/G_{\varepsilon,i}$ (−)
ε	porosity (−)
μ	liquid viscosity (Pa s)
v	short-hand for $k_e G_{\varepsilon,e}/\mu$ (m^2 s^{-1})
ξ	geometrical configuration constant relating α with k_i (−)
ρ	fluid density (g/m^3)
τ	characteristic time constant, short-hand for $\mu/\alpha G_{\varepsilon,i}$ (s)
v_{i-e}	rate of intra-to-extracellular liquid flux (s^{-1})

membranes (Ersus and Barrett, 2010). This selective property of pulsed electric fields makes electroporation an interesting process for enhancing juice extraction and dehydration, while preserving quality and organoleptic properties of juice and solids (Lebovka et al., 2004; Schilling et al., 2007).

Electroporation (also termed electropermeabilization) is a process where an externally applied electric field of sufficient strength induces a transmembrane potential, causing an increase in plasma membrane permeability and conductivity. This increase has been attributed to creation of aqueous pathways (pores) in the lipid bilayer, and has been demonstrated by experiments on lipid bilayers, cells in suspension, monolayers, and biological tissues. For essential reading in fundamentals of electroporation, see e.g. (Haberl et al., 2013; Kotnik et al., 2012; Krassowska and Filev, 2007; Neu and Neu, 2009).

In order to gain better understanding of the processes governing juice extraction and material consolidation behaviour in tissue electroporation, mathematical models can be constructed. These models need to be validated, before they are used to study the phenomena. The purpose of modelling can be, for instance, to facilitate optimization of industrial processes in terms of required energy or product quality (Bazhal et al., 2003; Schilling et al., 2007). However, due to the complexity and variability in properties of biological material and the many parameters and treatment effects on tissue, few complete and comprehensive models exist. Research in this direction is focused on modelling the mechanism of filtration–consolidation during pressing (Shirato et al., 1986; Lanoiselle et al., 1996; Zhu and Melrose, 2003; Petryk and Vorobiev, 2007, 2013; Halder et al., 2011), and less towards the electroporation-induced damage to the cell membranes. Even less is known, in terms of theory, about the effect of electroporation on permeability and compressibility of treated material. For a recent review of some of the fundamental concepts of applying porous media theory to mass transport in biological systems, see (de Monte et al., 2013).

In this article we aim to show how an extendable model can be constructed for describing filtration–consolidation behaviour of electroporated vegetable tissue. We have named this model the *dual-porosity model of liquid expression*. "Dual-porosity" since one porosity is that of the intercellular matrix of tissue, and the second the porosity of the plasma membrane of each individual tissue-constituting cell. We directly relate electroporation effects with important filtration–consolidation parameters, namely hydraulic permeability. We consider the intracellular and the extracellular space separately, and provide a theoretical approach to describe effects of electroporation on cell membrane hydraulic permeability. Theoretical analysis and fitting experimental data from pressing experiments are used as initial estimates for model parameter values, and then optimization algorithms were employed to fine-tune some of the parameters to obtain good agreement with experimental data. Tissue and membrane hydraulic permeability are estimated based on published literature where available, while compressibility moduli were estimated from analysis of pressing experiments that we conducted. We demonstrate how the proposed model can be used to model experimental extraction kinetics for both intact and electroporated tissue. We also provide a brief parametrical study. The model can easily be extended by a theoretical model of electroporation, and invites further development. By constructing the dual-porosity model we attempt to advance the field of modelling transport phenomena in electroporated biological tissues of industrial importance. A fully developed and validated model based on this approach could in future be used for research into optimization of treatment parameters, or for simulations of system responses under treatment conditions impractical or costly for realisation. The main novelty of the model in relation to previous works by our group is in connecting the theory of electroporation with the consolidation–filtration theory applied to study expression kinetics in biological tissues.

2. Theoretical formulation of the problem and derivation of an analytical model

2.1. System of liquid pressure equations in a dual-porosity medium

In order to study the expression of liquid from vegetable tissue treated with electroporation, we consider tissue as comprising two media – the intracellular, and the extracellular. The cell membrane on which electric field acts during electroporation delineates these two media in every tissue sample. The effects of electroporation on tissue permeability are introduced into the model via the membrane, by representing it as a semi-permeable boundary. The model membrane has its own hydraulic permeability, which is a function of electroporation. The extracellular space, represented as consisting of an intricate structure formed by the cell wall, extracellular liquid, and air (see Fig. 1), also has its own hydraulic permeability.

According to previous works based on filtration–consolidation theory of biosolids (Lanoiselle et al., 1996; Petryk and Vorobiev, 2007, 2013), the following set of equations can be written for the extracellular and intracellular space, respectively

$$\frac{\partial(\rho \varepsilon_e)}{\partial t} + \frac{\partial(\rho q_e)}{\partial z} - \rho v_{i-e} = 0 \tag{1}$$

$$\frac{\partial(\rho \varepsilon_i)}{\partial t} + \frac{\partial(\rho q_i)}{\partial z} + \rho v_{i-e} = 0 \tag{2}$$

Eqs. (1) and (2) result from application of the law of mass conservation, and are presented in a form typical for non-equilibrium mass transfer processes in porous media. In Eqs. (1) and (2), ρ is the liquid medium density; ε_e and ε_i are the porosities; q_e and q_i the liquid flow velocities; and v is the source term that represents the flow of liquid through the plasma membrane from the intracellular to the extracellular space. Indices 'i' and 'e' in Eqs. (1) and (2) correspond to the intracellular and the extracellular phase, respectively. The permeability of extracellular space is several orders of magnitude greater than that of intact cellular membrane (Buttersack and Basler, 1991; Tomos, 1988). This should still hold for tissue damaged by electroporation below the threshold that results in predominantly irreversible damage to the cell membranes. This is postulated in accordance with the theoretical derivations for permeability of electroporated cell membrane (see Section 2.5) and surface fraction of stable, long-lasting pores in the plasma membrane, as estimated in e.g. (Pavlin and Miklavcic, 2008). If treatment conditions support these assumptions, the liquid path is primarily from within the cells into the extracellular space and via compression of the extracellular space then out of the tissue block. Fig. 2 is in aid of illustrating the individual constituent
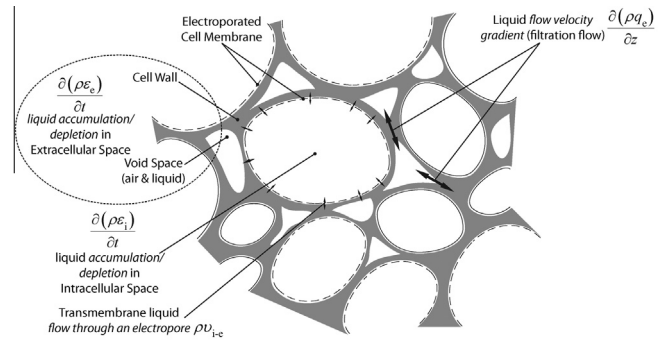

Fig. 2. A schematic representation of vegetable tissue after electroporation with identified member terms of the continuity Eqs. (1–2, also 3–4) in aid of illustrating the dual-porosity principle.

members of Eqs. (1) and (2), simplified by neglecting the filtration path through the intracellular space (see Eq. (4) below).

The experimental setup and a simplified representation of experiment physics are given in Fig. 3. The piston is applying pressure to the tissue in the –z direction, and liquid is flowing out of the tissue sample at $z = 0$, where a porous support (metallic mesh or filter cloth) is placed in order to hold the block of cellular tissue in place, while allowing free flow of extracted juice. The piston displacement during experiment is recorded, and the tissue block deformation can be calculated.

Assuming constant juice density ρ, and the supposition that filtration flow inside the cells can be neglected, Eqs. (1) and (2) simplify to

$$\frac{\partial \varepsilon_e(z,t)}{\partial t} + \frac{\partial q_e(z,t)}{\partial z} - v_{i-e}(z,t) = 0 \tag{3}$$

$$\frac{\partial \varepsilon_i(z,t)}{\partial t} + v_{i-e}(z,t) = 0 \tag{4}$$

We reformulate the above set of equations to express the quantities in terms of the two variables of known initial and boundary conditions, i.e. liquid pressures p_i and p_e. Pressure p_i is the intracellular liquid pressure, and p_e the extracellular liquid pressure. The porosities ε_e and ε_i are related to the solid pressures $p_{e,S} = P_E - p_e$ and $p_{i,S} = P_E - p_i$ via the compressibility moduli G_e and G_i, and the void ratios e_e and e_i, where $\varepsilon_e = e_e/(1 + e_e)$ and $\varepsilon_i = e_i/(1 + e_i)$. The relationships between void ratios and solid pressures are given by (Lanoiselle et al., 1996)

$$\frac{\partial e_e}{\partial t} = \frac{\partial e_e}{\partial p_{e,S}} \cdot \frac{\partial p_{e,S}}{\partial t} = -\frac{\partial e_e}{\partial p_{e,S}} \cdot \frac{\partial p_e}{\partial t} = \frac{1}{G_e} \frac{\partial p_e}{\partial t} \tag{5}$$
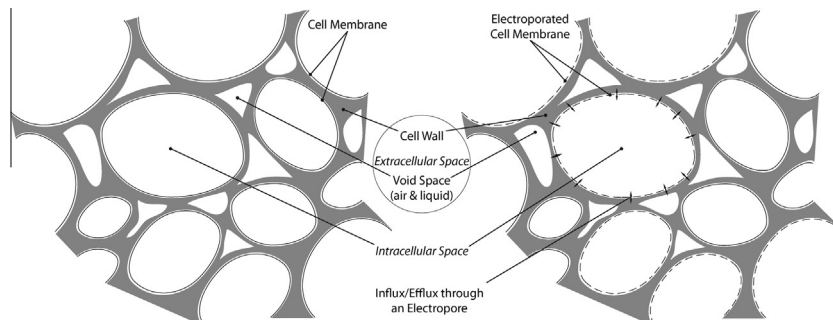

Fig. 1. A schematic representation of vegetable tissue before (left) and after (right) electroporation. The cell wall and void space, occupied by air and some liquid, are the solid and liquid phases forming the extracellular space in tissue (no external pressure applied). Redrawn based on Fig. 17 in Halder et al. (2011).
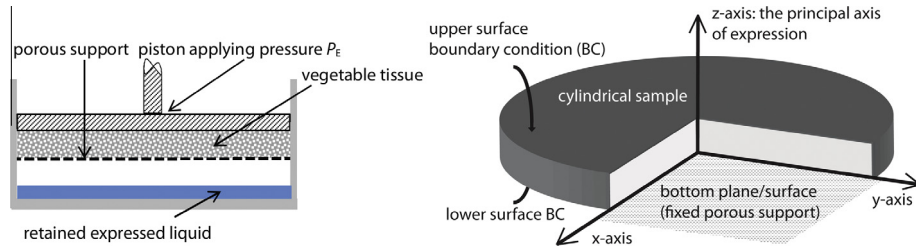
Fig. 3. A schematic representation of a typical pressing experiment (left) and a representation of the modelled block of tissue placed within a coordinate system (right).

$$\frac{\partial e_i}{\partial t} = \frac{\partial e_i}{\partial p_{i,S}} \cdot \frac{\partial p_{i,S}}{\partial t} = -\frac{\partial e_i}{\partial p_{i,S}} \cdot \frac{\partial p_i}{\partial t} = \frac{1}{G_i} \frac{\partial p_i}{\partial t} \qquad (6)$$

where $p_{e,S}$ and $p_{i,S}$ are the pressures of total insoluble solids in extracellular and intracellular phase, respectively. These solid pressures increase in time proportionally to the decrease in respective liquid pressures, i.e. $\partial p_{e,S}/\partial t = -\partial p_e/\partial t$ and $\partial p_{i,S}/\partial t = -\partial p_i/\partial t$. Note that this is valid for constant-pressure expression, when $\partial P_E/\partial t = 0$. From Eqs. (5) and (6) we see that G_e and G_i, if assumed constant, can be estimated from $G_e = -\partial p_{e,S}/\partial e_e$ and $G_i = -\partial p_{i,S}/\partial e_i$, i.e. the slopes of the linear functions that relate the decrease in void ratio with an increase in solid pressure. Note that G_e and G_i are always positive-value quantities, as an increase in solid pressure is a consequence of a decrease in void ratio (expression of liquid). In experiments, we measure the changes in deformation of the tissue sample due to loss of liquid, rather than measuring the liquid pressure. Therefore, we rewrite Eqs. (5) and (6) not for the liquid-to-solid void ratio, but for porosities ε_e and ε_i, as

$$\frac{\partial \varepsilon_e}{\partial t} = \frac{\partial p_{e,S}}{\partial t} \cdot \frac{\partial \varepsilon_e}{\partial p_{e,S}} = -\frac{\partial p_e}{\partial t} \cdot \frac{\partial \varepsilon_e}{\partial p_{e,S}} = \frac{1}{G_{\varepsilon,e}} \frac{\partial p_e}{\partial t} \qquad (7)$$

$$\frac{\partial \varepsilon_i}{\partial t} = \frac{\partial p_{i,S}}{\partial t} \cdot \frac{\partial \varepsilon_i}{\partial p_{i,S}} = -\frac{\partial p_i}{\partial t} \cdot \frac{\partial \varepsilon_i}{\partial p_{i,S}} = \frac{1}{G_{\varepsilon,i}} \frac{\partial p_i}{\partial t} \qquad (8)$$

The compressibility moduli G_e and G_i as defined in cited literature and $G_{\varepsilon,e}$ and $G_{\varepsilon,i}$ defined in Eqs. (7) and (8) are related, as follows from the relations

$$\frac{\partial \varepsilon_e}{\partial t} = \frac{\partial p_{e,S}}{\partial t} \cdot \frac{\partial}{\partial p_{e,S}}\left(\frac{e_e}{1+e_e}\right) = -\frac{\partial p_e}{\partial t} \cdot \frac{\partial e_e}{\partial p_{e,S}} \frac{1}{(1+e_e)^2}$$
$$= \frac{1}{G_e} \frac{1}{(1+e_e)^2} \frac{\partial p_e}{\partial t} = \frac{1}{G_{\varepsilon,e}} \frac{\partial p_e}{\partial t} \qquad (9)$$

$$\frac{\partial \varepsilon_i}{\partial t} = \frac{\partial p_{i,S}}{\partial t} \cdot \frac{\partial}{\partial p_{i,S}}\left(\frac{e_i}{1+e_i}\right) = -\frac{\partial p_i}{\partial t} \cdot \frac{\partial e_i}{\partial p_{i,S}} \frac{1}{(1+e_i)^2}$$
$$= \frac{1}{G_i} \frac{1}{(1+e_i)^2} \frac{\partial p_i}{\partial t} = \frac{1}{G_{\varepsilon,i}} \frac{\partial p_i}{\partial t} \qquad (10)$$

According to the Eqs. 9–10, $G_{\varepsilon,e} = G_e \cdot (1 + e_e)^2$ and $G_{\varepsilon,i} = G_i \cdot (1 + e_i)^2$. By introducing compressibility moduli defined through porosity, we have made a simplification that comes at a cost. The $G_{\varepsilon,e}$ and $G_{\varepsilon,i}$ do not depend only on material properties and treatment, but also on the spatially- and temporally-dependent void ratios e_e and e_i during the pressing experiment. This is a trade-off we have opted for in order to keep the model simple and comprehensive. As a consequence, the model results are valid for small piston displacements in cases where tissue is not severely damaged. The moduli $G_{\varepsilon,e}$ and $G_{\varepsilon,i}$ that we use, should be understood as averaged values, i.e.

$$\overline{G}_{\varepsilon,e} = G_e(1+\bar{e}_e)^2 = G_e\left(1 + \frac{1}{T}\frac{1}{h}\int_0^h\int_0^T e_e(z,t) \cdot dt \cdot dz\right)^2 \qquad (11)$$

$$\overline{G}_{\varepsilon,i} = G_i(1+\bar{e}_i)^2 = G_i\left(1 + \frac{1}{T}\frac{1}{h}\int_0^h\int_0^T e_i(z,t) \cdot dt \cdot dz\right)^2 \qquad (12)$$

where T is the time duration of the experiment and h is the initial sample height. We omit the bar notation denoting average values in the following text. The minimum values of compressibility moduli can be directly estimated from experiments (see Section 2.4, where parameter estimation is presented), and average values as given by Eqs. (11) and (12), will be determined based on fitting of model results to experimental data. Another simplification limiting model applicability to small piston displacements is the assumption of linear elastic deformation of tissue. Compressibility moduli $G_{\varepsilon,e}$ and $G_{\varepsilon,i}$ are, more strictly following definitions of thermodynamics and stress mechanics, in fact non-normalized bulk elastic moduli. A more in-depth and rigorous treatment in filtration-consolidation theory would require introduction of material coordinates $dz_m = (1 - \varepsilon) \cdot dz$ (Petryk and Vorobiev, 2013) to account for time and space-variable porosity.

The liquid flow velocity in extracellular space q_e is given by Darcy law as

$$q_e = -\frac{k_e}{\mu}\frac{\partial p_e}{\partial z}, \qquad (13)$$

assuming unidirectional flow in direction of the principal axis of applied pressure (z).

The source term $v_{i-e}(z,t)$ giving liquid flow through the porous membrane can be written in terms of local pressure difference between the intracellular and extracellular liquid pressure, giving

$$v_{i-e} = \frac{\alpha}{\mu}(p_i - p_e) \qquad (14)$$

wherein we notice the proportionality coefficient α, whose origin and estimation are discussed in Section 2.4.

Combining Eqs. 3–14 and dropping the notation of spatial–temporal dependency of both liquid pressures gives the following final form of the model equations:

$$\frac{1}{G_{\varepsilon,e}}\frac{\partial p_e}{\partial t} - \frac{\partial}{\partial z}\left(\frac{k_e}{\mu}\frac{\partial p_e}{\partial z}\right) - \frac{\alpha}{\mu}(p_i - p_e) = 0 \qquad (15)$$

$$\frac{1}{G_{\varepsilon,i}}\frac{\partial p_i}{\partial t} + \frac{\alpha}{\mu}(p_i - p_e) = 0 \qquad (16)$$

The initial and boundary conditions for Eqs. (15) and (16) are

$$p_{e0} = p_{e0}(z,0) = p_{i0} = p_{i0}(z,0) = P_E \qquad (17)$$

$$p_e|_{z=0} = 0 \qquad (18)$$

$$p_i|_{z=0} = p_{i0}e^{-\frac{\alpha G_i}{\mu}t} \qquad (19)$$

$$\left.\frac{\partial p_e}{\partial z}\right|_{z=h} = \left.\frac{\partial p_i}{\partial z}\right|_{z=h} = 0 \qquad (20)$$

The boundary condition given by Eq. (19) can be obtained by solving Eq. (16) for the boundary condition given in Eq. (18) and initial condition in Eq. (17). As the matter is trivial, we leave the details of verifying Eq. (19) to the interested reader. A note on initial condition, Eq. (17); Externally applied pressure can be assumed as equally distributed throughout the tissue sample on both the intra- and extracellular liquid phase in case the sample thickness is relatively small (in relation to the number of cell layers and piston-tissue contact surface). If the sample thickness impact to pressure distribution cannot be neglected due to sample dimensions, a more suitable approximation for pressure distribution might be linear, for details, see e.g. (Lanoiselle et al., 1996). In experiments we performed, the conditions (use of thin samples) justify applicability of this initial condition. This is consistent with consolidation theory of porous material mechanics (Šuklje, 1969). We also suppose that pressure P_E redistributes itself equally onto the liquid phase of both the extracellular (p_{e0}) as well as the intracellular space (p_{i0}) at the beginning of a pressing experiment, after the extracellular air is eliminated and replaced by liquid at the beginning of the consolidation stage (Lanoiselle et al., 1996).

2.2. Analytical solution for liquid pressure

We give the analytical solution of PDEs Eqs. (15) and (16) for initial and boundary conditions Eqs.(17)–(20). The mathematical details of the derivation can be found for the case of an analogous problem of solute diffusion in electroporated tissue, given in full details in our recent publication (Mahnič-Kalamiza et al., 2014). For brevity, we only give the solution in final form below.

The intracellular liquid pressure p_i can be expressed as

$$p_i(z,t) = \frac{4p_{i0}}{\pi} \sum_{n=0}^{\infty} \frac{1}{2n+1} (C_1 e^{\gamma_{n,1}t} + C_2 e^{\gamma_{n,2}t} - e^{-\tau^{-1}t}) \sin\left(\frac{(2n+1)\pi}{2h}z\right) + p_{i0} e^{-\tau^{-1}t} \tag{21}$$

where

$$C_1 = \frac{\left(\frac{p_{e0}}{p_{i0}} - 1\right)\tau^{-1} - \gamma_{n,2}}{\gamma_{n,1} - \gamma_{n,2}}, \tag{22}$$

$$C_2 = \frac{\left(1 - \frac{p_{e0}}{p_{i0}}\right)\tau^{-1} + \gamma_{n,1}}{\gamma_{n,1} - \gamma_{n,2}} \tag{23}$$

and

$$\gamma_{n_{1,2}} = \frac{-(\tau^{-1}\delta + \lambda_n^2 v) \pm \sqrt{(\tau^{-1}\delta + \lambda_n^2 v)^2 - 4\lambda_n^2 v\tau^{-1}}}{2}, \tag{24}$$

where for the sake of algebra we have set

$$v = \frac{k_e G_{\varepsilon,e}}{\mu}; \quad \tau^{-1} = \frac{\alpha G_{\varepsilon,i}}{\mu}; \quad \delta = \left(1 + \frac{G_{\varepsilon,e}}{G_{\varepsilon,i}}\right); \quad p_{i0} = p_i(z,0);$$
$$p_{e0} = p_e(z,0).$$

The eigenvalues λ_n equal $\lambda_n = (2n+1)/2 \cdot \pi/h$.
For extracellular liquid pressure p_e, we have

$$p_e(z,t) = \frac{4p_{i0}}{\pi} \sum_{n=0}^{\infty} \frac{1}{2n+1} ((\gamma_{n,1}\tau + 1)C_1 e^{\gamma_{n,1}t} + (\gamma_{n,2}\tau + 1)C_2 e^{\gamma_{n,2}t}) \sin\left(\frac{(2n+1)\pi}{2h}z\right) \tag{25}$$

where all coefficients are calculated according to expressions already defined for intracellular pressure.

The infinite series in Eq. (21), as can easily be verified, converges extremely rapidly, even if few members of the infinite series are taken for summation. On the contrary, the series in Eq. (25) is more demanding and converges slowly, as it has to approximate the discontinuity present at $z = 0$, where the extracellular pressure

drops immediately from the constant (initial condition) value to 0. In practice though, it is far more efficient in computational terms to not use Eq. (25), but calculate $p_i(z,t)$ according to Eq. (21). As few as 3–5 members of the series suffice to achieve accuracy required by most practical applications. Once the intracellular pressure is known, we can use relation given by the following equation, which has been rewritten by expressing p_e from Eq. (16)

$$p_e = \frac{\mu}{\alpha G_{\varepsilon,i}} \frac{\partial p_i}{\partial t} + p_i \tag{26}$$

to numerically calculate the extracellular pressure $p_e(z,t)$, which is a matter of numerical derivation and some arithmetic. The calculation of both pressures on an average modern laptop computer using the software package MATLAB (MathWorks, Massachusetts, USA) and employing an algorithm based on Eqs. (21) and (26) as described above, requires between 10 and 20 ms for a spatial and temporal resolution of 100 nodes. This makes the model suitable for use in optimization algorithms, and is one of the reasons why we opted for model simplification and derivation of a relatively simple analytical solution, rather than computing liquid pressures numerically.

Another advantage of the analytical solution is it provides the possibility for analysing model behaviour. From Eqs. (21) and (25), we can determine that process kinetics is governed entirely by the roots of the characteristic polynomial (given by Eq. (24)). If there is no electroporation and $\tau^{-1} \to 0$, Eq. (24) can be simplified and gives $\gamma_{n,1} \to 0$ and $\gamma_{n,2} \to -\lambda_n^2 v$. At these conditions, expression–consolidation kinetics is governed entirely by the rate of expression through extracellular space, i.e. k_e, and there is no transmembrane flow (since $\tau^{-1} \to 0$). Eq. (1) becomes an ordinary one-dimensional filtration–consolidation equation. We should point out that the analytical solution given by Eqs. (21) and (25) becomes extremely unstable for numerical evaluation when $\tau^{-1} \to 0$. As τ^{-1} decreases, numerical errors due to finite machine precision (32- or 64-bit floating point representation and operations) are amplified and the model results become unstable. For machine precision on the order of 10^{-16}, this effect becomes observable around $\tau^{-1} = 10^{-14}$ and the results become completely unusable for $\tau^{-1} < 10^{-15}$. At these extreme conditions however, there is no justification for use of the dual-porosity model whatsoever, and analysis of filtration–consolidation behaviour in extracellular space can be better described by a simpler model.

At the other extreme, for highly electroporated tissue ($f_p \to 1$, see Section 2.5 for the definition), for f_p values above approximately 10^{-3}, the membrane appears to disintegrate, i.e. to lose its barrier function for liquid flow. In Eq. (24) we then have $\tau^{-1}\delta \gg \lambda_n^2 v$. This results in extremely rapid kinetics ($|\gamma_2| \approx \tau^{-1}\delta \gg 1$) of transmembrane filtration and instantaneous expression of liquid from the intracellular into the extracellular space, provided there is a liquid pressure gradient. This is again unrealistic and outside the scope of the model, as the intracellular filtration pathway is not captured by model equations. The other exponential however, $C_1\exp(\gamma_1 t)$, is governed primarily by k_e, which limits vacation of liquid out of the tissue block via the extracellular space. Since $C_1 \gg C_2$ this results in almost identical expression–consolidation kinetics in extracellular space as in non-electroporated tissue, but with comparatively higher extracellular liquid pressure at a given time. This is expected, since the extracellular space has to facilitate vacation of not only the liquid initially present in the extracellular phase, but of the liquid initially present within the cells as well.

As emphasized during the analysis, there are limitations of the proposed dual-porosity model and its analytical solution, in addition to those already discussed in connection with the compressibility moduli. These limitations must be kept in mind during

experimentation with the model, and one should maintain a critical outlook on the results in light of these observations to avoid analysis under unrealistic or extreme conditions. We will further comment on the issue in the Results section.

2.3. Model application – from theory to experimentally measured kinetics

In pressing experiments set up as shown schematically in Fig. 3, the quantity observed is most commonly the deformation of the sample block of tissue (Grimi et al., 2010; Mhemdi et al., 2012). Our model thus far concerns liquid pressures in the extracellular and intracellular space. In order to compare model results with experiments, we must find an expression giving deformation as a function of the cumulative change of pressure throughout the sample. The relationship between loss of liquid pressure and deformation is already given by Eqs. (5) and (6). Since total deformation is the sum of deformation of extracellular and of intracellular space, we have

$$S(t) = S_e(t) + S_i(t), \tag{27}$$

Total deformation can be expressed as a spatial integral of local infinitesimal differences in void ratio e, therefore

$$S(t) = \int_0^h \int_{e_e(z,t)}^{e_e(z,0)} de_e \cdot dz + \int_0^h \int_{e_i(z,t)}^{e_i(z,0)} de_i \cdot dz$$
$$= \frac{1}{G_e} \int_0^h \int_{p_e(z,t)}^{p_e(z,0)} dp_e \cdot dz + \frac{1}{G_i} \int_0^h \int_{p_i(z,t)}^{p_i(z,0)} dp_i \cdot dz. \tag{28}$$

Since we are working with porosity ε instead of void ratio e, and for reasons of convenience, we define relative deformation s_ε

$$s_\varepsilon(t) = \frac{S_\varepsilon(t)}{h}$$
$$= \frac{1}{G_{\varepsilon,e}} \int_0^1 \int_{p_e(z,t)}^{p_e(z,0)} dp_e \cdot dz + \frac{1}{G_{\varepsilon,i}} \int_0^1 \int_{p_i(z,t)}^{p_i(z,0)} dp_i \cdot dz, \tag{29}$$

where h is the tissue sample height. Eq. (29) gives relative deformation as a function of loss of liquid pressure within the tissue. We will use it to obtain model results and compare them with experimental data.

2.4. Estimation of permeability and compressibility coefficients

2.4.1. Compressibility moduli $G_{\varepsilon,e}$, $G_{\varepsilon,i}$
We imagine two experimental scenarios. In the first experiment, freshly cut intact tissue is subjected to pressing under pressure of insufficient strength to cause cell rupture. Under these conditions, when equilibrium between the pressure applied via piston and the intracellular liquid pressure is reached (neglecting the extracellular solid pressure), we will have obtained a certain measurable but small deformation. If the pressure applied is sufficient to completely express extracellular fluid while not compromising the integrity of the cell plasma membrane, this measured deformation is only due to the compression of extracellular space. We write

$$s_{e,\infty} = s_e(t \to \infty) = \frac{1}{G_{\varepsilon,e}} \int_0^1 \int_{p_e(z,t \to \infty)}^{p_e(z,0)} dp_e \cdot dz$$
$$= \frac{1}{G_{\varepsilon,e}} \int_0^1 \int_0^{P_E} dp_e \cdot dz = \frac{P_E}{G_{\varepsilon,e}} \tag{30}$$

Eq. (30) provides means to estimate $G_{\varepsilon,e}$ directly from pressing experiments done on intact, untreated (non-electroporated) tissue. With known deformation at "infinite" time and known applied pressure P_E, we have

$$G_{\varepsilon,e} \cong \frac{P_E}{s_{e,\infty}}. \tag{31}$$

Since $G_{\varepsilon,e}$ is a function of void ratio, which is not constant in time (and is only approximately constant throughout the tissue block along z, provided the sample is thin), the value obtained by Eq. (31) is a rough initial estimate, and a good approximation for untreated tissue only. It is expected to decrease with increasing treatment intensity, since it is not a material property but depends on e. We will have to determine the average value (as defined by Eq. (11)) by optimization against experiments.

We propose another conceptual experiment for estimating $G_{\varepsilon,i}$. If we permeabilize the cell membranes (by e.g. electroporation), under applied pressure liquid will flow from intracellular to extracellular space and through the latter out of the tissue block. At complete equilibrium (i.e. after "infinite" time), all liquid will be expressed from the sample, and the externally applied pressure will be balanced by the sum of solid pressures of intracellular and extracellular space. We write

$$s_\infty = s_e(t \to \infty) + s_i(t \to \infty)$$
$$= \frac{1}{G_{\varepsilon,e}} \int_0^1 \int_{p_e(z,t \to \infty)}^{p_e(z,0)} dp_e \cdot dz + \frac{1}{G_{\varepsilon,i}} \int_0^1 \int_{p_i(z,t \to \infty)}^{p_i(z,0)} dp_i \cdot dz$$
$$= \frac{1}{G_{\varepsilon,e}} \int_0^1 \int_0^{P_E} dp_e \cdot dz + \frac{1}{G_{\varepsilon,i}} \int_0^1 \int_0^{P_E} dp_i \cdot dz = \frac{P_E}{G_{\varepsilon,e}} + \frac{P_E}{G_{\varepsilon,i}}$$
$$= \frac{P_E(G_{\varepsilon,i} + G_{\varepsilon,e})}{G_{\varepsilon,e}G_{\varepsilon,i}} \tag{32}$$

If $G_{\varepsilon,e}$ is known, e.g. determined according to Eq. (31), and we measure deformation in an experiment with strongly permeabilized tissue, by expressing $G_{\varepsilon,i}$ from Eq. (32), we get

$$G_{\varepsilon,i} \cong \frac{P_E G_{\varepsilon,e}}{s_\infty G_{\varepsilon,e} - P_E}, \tag{33}$$

which is a function of either previously known or measurable parameters. This estimate gives an approximate value for $G_{\varepsilon,i}$ in case of damaged tissue. The average value (as per Eq. (12)) for untreated or only moderately electropermeabilized tissue is expected to be much higher. As with $G_{\varepsilon,e}$, the value corresponding to the particular degree of electropermeabilization will be determined by fitting model results to experimental data.

2.4.2. Intrinsic hydraulic permeabilities k_e and k_i
Hydraulic permeability of tissue is almost always measured rather than calculated (Buttersack and Basler, 1991), due to high complexity of water pathways within tissue that makes theoretical estimates hard to obtain, and the biological diversity, which renders these estimates unreliable across different plant species and across samples of a single species. Measurements on a number of plant tissues and yeast cells show a wide range of values for permeability, spanning several orders of magnitude, for both tissue as well as plasma membrane of individual cells (Buttersack and Basler, 1991; Tomos, 1988).

This paper is concerned with juice expression from untreated and electroporated sugarbeet. Since sugarbeet is of great industrial importance, it is one of the few crop species that have been more extensively studied in terms of its water transport and consolidation properties. In literature, it is possible to find several accounts of measurement of hydraulic conductivity (L_p) of sugarbeet roots and cells comprising the root tissue. Here, we demonstrate how it is possible to recalculate these measurements in order to estimate the intrinsic hydraulic permeability coefficients required by our model.

The hydraulic conductivity L_p found in literature is normally calculated based on an experiment where a tissue sample is sub-

jected to a pressure difference and liquid volume flux is measured. With known flux and pressure, the hydraulic conductivity is

$$L_p = \frac{q}{\Delta p}. \tag{34}$$

On the other hand, the Darcy law relates the pressure drop across a conduit of length l with the liquid flux q as

$$|q| = \frac{k}{\mu} \frac{\Delta p}{l}. \tag{35}$$

Note that we write the absolute value of q since we are not interested in the direction of the flow. Inserting q from Eq. (34) into Eq. (35) and expressing k gives

$$k = L_p \cdot \mu \cdot l. \tag{36}$$

Eq. (36) can be used to calculate the intrinsic hydraulic permeability of tissue from measurements obtained via experiments described above. For instance, Amodeo et al. (Amodeo et al., 1999) measured conductivity of 3 mm slices (osmotic flow length l) of untreated sugarbeet roots in the axial and radial direction, obtaining in the radial direction (perpendicular to the major water transport channels) a conductivity of $5\cdot10^{-6}$ m MPa^{-1} s^{-1}. Using Eq. (31) and water viscosity of 10^{-3} Pa s, we obtain (for $l = 3$ mm) $k = 1.5\cdot10^{-17}$ m^2. Assuming negligible symplastic flow (i.e. only apoplastic), this is the sought hydraulic permeability of extracellular space, k_e.

The intracellular hydraulic permeability k_i is in fact the hydraulic permeability of the plasma membrane of thickness l. This coefficient is expected to change when treatment, be it mechanical, thermal, chemical, enzymatic or electrical, is applied to the tissue. Its initial value (i.e. for untreated tissue) can be estimated from pressure-probe experiments. Tables of cell membrane hydraulic permeability are given in literature for many plant and yeast species, including sugarbeet. In (Tomos, 1988) we find for hydraulic conductivity of sugarbeet cell membrane the value of $0.2\cdot10^{-6}$ m MPa^{-1} s^{-1}. Given a membrane thickness of 5 nm, Eq. (36) yields membrane intrinsic hydraulic permeability $k_i = 10^{-24}$ m^2.

2.5. Electroporation effects on plasma membrane permeability – the proportionality coefficient α

The proportionality coefficient α (dimensionless) proposed in the model definition (Eq. (14)), relates the intracellular and extracellular deformation due to transmembrane flux with the pressure drop across the plasma membrane. It needs to be, according to model design and assumptions, a function of membrane permeability k_i, multiplied by a corrective geometrical factor ξ with units m^{-2}. This corrective factor ξ accounts for the geometrical configuration of the cell and its porous membrane by relating intracellular space porosity with volume-averaged transmembrane flux (further explanation can be found in the Appendix). For negligible membrane thickness as compared to the size of the cell, ξ equals the square of specific surface (surface-to-volume ratio), i.e. $\xi = (A/V)^2$. On the level of a biological cell, where transmembrane fluid transport occurs, the surface A and volume V are those of a single cell. For an idealized, average, spherical cell of sugarbeet tissue with a radius of 25 μm (Buttersack and Basler, 1991), the corrective factor ξ equals $1.44\cdot10^{10}$. Consequently, the proportionality coefficient α is written as $\alpha = 1.44\cdot10^{10}\cdot k_i$. For a detailed theoretical derivation which is also applicable in cases where membrane is not of negligible thickness, see the Appendix.

We now turn to the effect of electroporation treatment on the hydraulic permeability coefficient, k_i. According to the theory of electroporation (Neu and Neu, 2009; Kotnik et al., 2012; Haberl et al., 2013), electric field of sufficient strength creates pores in the plasma membrane. These pores nucleate at an initial radius of about 0.5 nm, and can expand in both number and size during the application of electric field. The effect has a transient as well as a long-lasting component, i.e. transient and long-lasting pores are created in the membrane (Pavlin and Miklavcic, 2008). It has been demonstrated by several experiments, see e.g. (Saulis and Saule, 2012), that long-lasting pores permeable to molecules of e.g. bleomycin (about 1.6 nm in diameter) or sucrose (0.44–0.52 nm diameter), can exist in an electroporated membrane for minutes after the application of electric pulses, though they are subject to resealing if physiological conditions are favourable. We can, assuming an average stable pore diameter and pore fraction ratio (i.e. the surface fraction of all pores per one cell), estimate how electroporation changes the hydraulic permeability of the cell membrane.

We start by relating membrane permeability k_i with permeability of a single aqueous pore. The absolute value of membrane flux is, according to Darcy law,

$$|Q_m| = \frac{k_i A_m}{\mu} \frac{\Delta p}{l}, \tag{37}$$

but it is also the sum of all single-pore fluxes, of which there are as many as there are pores, i.e. N_p. We write

$$|Q_m| = N_p|Q_p| = \frac{N_p k_p A_p}{\mu} \frac{\Delta p}{l}. \tag{38}$$

From equating transmembrane flux in Eqs. (37) and (38) we obtain the relation

$$k_i = \frac{N_p k_p A_p}{A_m} = f_p k_p, \tag{39}$$

where $f_p = N_p A_p/A_m$ is the pore surface fraction.

According to literature (Pavlin and Miklavčič, 2008), surface fraction of long-lasting pores in B16F1 (mouse melanoma) cells for 8 pulses of 100 μs duration and strength of 1 kV/cm is on the order of $0.5\cdot10^{-5}$. In experiments with electroporation treatment of vegetable tissue for enhancing liquid extraction by pressing, many more pulses are normally used (100, 1000 or more), and cells in treated tissue can measure more than 10 times the size of cells in animal cell lines used most often in electroporation studies (i.e. Chinese hamster ovary – CHO, mouse melanoma – B16F1, etc.). Therefore, the upper limit of the range into which long-lasting pore fraction is expected to fall should be generously increased. Extrapolating results published in (Pavlin and Miklavčič, 2008), where a similar treatment protocol to ours was used, places the initial estimate for f_p at around $2\cdot10^{-5}$. However, this value must be understood as a highly unreliable estimate, as various phenomena involved in pore formation and stabilization were not accounted for (e.g. media conductivity, cell suspension vs. biological tissue, differences in cell size, etc.). Optimization with model results to fit experimental data in our model study resulted in estimates of pore surface fraction an order of magnitude higher (see Table 2, Section 3.1) as compared to the initial estimate. One possible reason we can suggest to explain this discrepancy is the much higher induced transmembrane voltage in large plant cells (our study) as opposed to smaller animal cells (cited reference). According to electroporation theory, pore surface fraction is strongly dependent on induced transmembrane voltage. More work should be dedicated to determining the parameters that describe membrane long-term permeability with respect to the treatment protocol. More specifically, if the radius of an average stable pore is underestimated – and due to persistence of large pores several minutes after pulse application it most probably is (Saulis and Saulė, 2012) – the resulting pore surface fraction according to pressing experiments will be overestimated, as higher surface fraction will compensate for the lower single pore hydraulic permeability.

Table 1
Expressions for model parameter estimations – a summary.

Parameter	Value	Method
$G_{\varepsilon,e}$	P_E/s_∞	From experiments
$G_{\varepsilon,i}$	$\dfrac{P_E G_{\varepsilon,e}}{s_\infty G_{\varepsilon,e} - P_E}$	From pressing experiments
k_e	$L_p \cdot \mu \cdot l$	Osmotic flow measurements (l is tissue sample thickness)
k_i	$L_p \cdot \mu \cdot l$	Pressure probe measurements (l is membrane thickness)
k_p	$r_p^2/8$	Hagen-Poiseuille theoretical estimation
$k_{i,EP}$	$\dfrac{N_p k_p A_p}{A_m} = f_p k_p$	Theoretical estimation (k_p) and estimate based on fitting the model to experimental data (f_p)
α	$k_i \cdot (A/V)^2$	Theoretical estimate based on pressure probe measurements
α_{EP}	$k_{i,EP} \cdot (A/V)^2$	Theoretical estimate based on fitting the model to experimental data

Table 2
Parameters used to obtain model results, simulation results are plotted against experiments in Fig. 4.

Parameter	Value	Method/source
P_E	5.82×10^5 Pa	As used in experiments
G_{e0} (initial estimate)	129×10^5 Pa	From final deformation of intact tissue – experiments
G_{i0} (initial estimate)	8×10^5 Pa	Recalculated from final deformation of electroporated tissue given known G_{e0} – experiments
G_{e0} (optimized)	130×10^5 Pa	Optimization using experimental results
G_{i0} (optimized)	16×10^5 Pa	Optimization using experimental results
k_{e0} (initial estimate)	1.5×10^{-17} m^2	Osmotic flow measurements (Amodeo et al., 1999)
k_e (optimized)	3.75×10^{-17} m^2	Optimization using experimental results
k_{i0} (initial estimate)	10^{-24} m^2	Pressure probe measurements (Tomos, 1988)
k_i (optimized)	10^{-24} m^2	Optimization using comparison with experimental results ($k_i = f_p \cdot k_p$)
$k_{i,EP}$ (optimized, at 400 V, Protocol A)	2.8×10^{-23} m^2	Optimization using comparison with experimental results ($k_i = f_p \cdot k_p$)
k_p	1.25×10^{-19} m^2	Hagen-Poiseuille theoretical estimation based on estimated average stable pore size
f_{p0}	2.5×10^{-5}	Extrapolation of experimentally-obtained estimates (Pavlin and Miklavčič, 2008)
f_p (optimized, at 400 V, Protocol A)	2.22×10^{-4}	Optimization using comparison with experimental results
α	1.44×10^{-10} m^{-2} k_i	Theoretical estimate for $\xi = 1.44 \times 10^{-10}$ m^{-2}, k_i from pressure-probe experiments
α_{EP}	1.44×10^{-10} m^{-2} $k_{i,EP}$	Theoretical estimate for $\xi = 1.44 \times 10^{-10}$ m^{-2}, $k_{i,EP}$ from experiments and pore size/population estimates (see f_p and k_p)

The remaining parameter to be estimated is the single pore intrinsic hydraulic permeability, k_p. To that end, we use the Hagen–Poiseuille equation for cylindrical pores of length l and radius r_p in combination with Darcy law. We get

$$\Delta p = \frac{8\mu l Q_p}{\pi r_p^4} = \frac{8\mu l Q_p}{r_p^2 A_p} = \frac{\mu l Q_p}{k_p A_p}. \tag{40}$$

From Eq. (40) k_p can be expressed as $r_p^2/8$. We now assume that the average size of a stable pore can be estimated from models of pore evolution during and after treatment, such as those reviewed by Saulis (Saulis, 2010). If we remain conservative, and suppose an average pore radius of about 1 nm with lifetime of minutes up to hours after treatment, k_p equals $1.25 \cdot 10^{-19}$ m^2. This gives for membrane (and intracellular space) permeability in electroporated tissue $k_{i,EP}$ the value of $2.7 \cdot 10^{-23}$, which is about 30-times higher than what has been estimated for intact cellular membrane, and can be found in literature (Tomos, 1988). The cited estimate is based on one particular study utilising a pressure probe technique, available only to the author of the cited review as an unpublished manuscript. We are therefore unable to analyse the methodology and calculations to evaluate the reliability and accuracy of this estimate. Parameter estimations are summarized in Table 1. Note that the model tissue under consideration is sugarbeet.

3. Results and discussion

3.1. Modelling experimental extraction kinetics for model validation

In order to demonstrate how the proposed model can be used in practice to explain experimentally-obtained kinetics, we present a comparison between experimental data obtained by pressing cylindrical sugarbeet slices, and the model simulation results. All parameters were initially estimated as described in the preceding

sections, and kept constant, except for the two compressibility moduli $G_{\varepsilon,e}$ and $G_{\varepsilon,i}$, the pore surface fraction of electroporated tissue f_p, and the extracellular permeability coefficient k_e. These parameters were sought for by means of optimization against the experimental data, with estimates (obtained via methods in Table 1) used as initial guesses. Using an optimization search to correct the values of these parameters is justified by the fact their estimate is prone to inaccuracy due to biological variability, and the compromises we made in theory to keep the model simple. We have however managed to remain well within one order of magnitude difference between the initial guess and the optimized value, suggesting the methods used for estimation are fairly reliable.

Fig. 4 below shows relative tissue sample deformation as a function of time. The simulated expression curves were obtained using parameters summarized in Table 2. Compressibility moduli were first estimated from modelled experiments as explained in
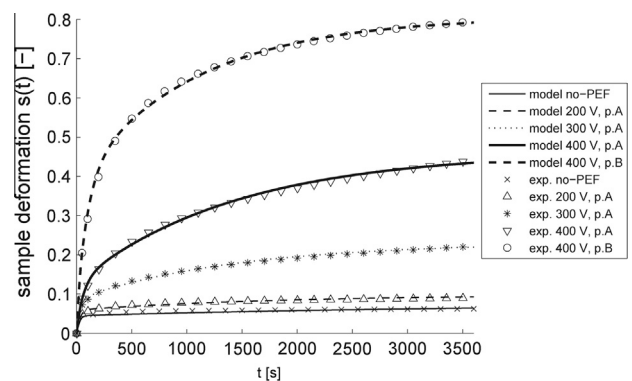

Fig. 4. Experimental data and model results. An optimization using RMSE as a criterion function was run to determine the parameters resulting in the best fit. Note that "p.A" stands for Protocol A and "p.B" for Protocol B.

Section 2.4.1, and then an optimization search for global minima of RMSE between experimental and model data was used to identify optimal values. The total relative deformation calculation follows Eq. (29) based on liquid pressures calculated using Eqs. (21) and (26). Detailed descriptions of the experimental setup used for data acquisition have previously been published in literature (Grimi et al., 2010). In short; we used cylindrical samples of sugarbeet tissue, 25 mm in diameter and 5 mm thick. The samples were placed between two parallel plate electrodes, and electroporation pulses were applied using two protocols. Protocol A: The voltage was varied, using 200 V, 300 V or 400 V applied to the electrodes. Bipolar pulses were delivered in two trains of 8 pulses per train, with repetition frequency of 1 kHz within the train, 1 s pause between the two trains, and 100 μs pulse duration. Protocol B: The voltage was fixed at 400 V, 20 unipolar pulses of 1 ms duration were applied with repetition frequency of 0.5 Hz. In all cases, regardless of the electroporation protocol, the electric treatment was followed by pressing. Electroporated samples were immediately placed into a specially fabricated treatment cell and subjected to a load of 300 N using a texturometer. The piston displacement was recorded by the texturometer under constant pressure application during one hour.

To fit experimental results, parameter f_p had to be increased from $8.0 \cdot 10^{-6}$ for untreated tissue to $2.0 \cdot 10^{-5}$ for the electrode voltage of 200 V; further to $9.5 \cdot 10^{-5}$ for 300 V; and finally to $2.2 \cdot 10^{-4}$ for 400 V (Protocol A). In case of treatment according to Protocol B at 400 V, f_p had to increase only slightly as compared to Protocol A at the same voltage, to $3.3 \cdot 10^{-4}$. This is consistent with electroporation theory and observations; pore surface fraction is a function of maximal electric field strength (Pavlin and Miklavcic, 2008). What had to be significantly altered comparing Protocol A at B at 400 V were the compressibility moduli and k_e. This was expected, as compressibility moduli reflect the extent of the bulk tissue damage (fraction of permeabilized cells), and in highly electroporated tissue, additional liquid paths (increase in k_e) should be created by vacant cell compartments of destroyed cells. One surprising and unexpected observation is the highly significant difference in compressibility modulus of the extracellular space, especially when comparing tissue treated with 400 V pulses and two different Protocols, A and B. This marked discrepancy cannot be explained as resulting from model (over)simplifications. The theory of electroporation however does offer a plausible explanation; Electroporation is a threshold phenomenon. Depending on the treatment parameters, a cell remains either undamaged, is reversibly permeabilized (and recovers if conditions are favourable), or is irreversibly electroporated. Irreversibly electroporated cells lose the ability to control transmembrane liquid and solutes flow. From the porous medium point of view, they can no longer be regarded as intracellular space. From this perspective, irreversible electroporation is responsible for transformation of the intra- to the extracellular phase; it is modifying the volumetric ratio of intra- and extracellular space, i.e. the volume fraction of cells. For field strengths and protocols that result in irreversible electroporation, we must take these effects into account, as the transmembrane filtration law (source term $v_{i-e}(z,t)$ in Eqs. (1) and (2), governed by f_p) cannot describe behaviour of irreversibly damaged membranes. This suggests that future model development should head towards coupling the filtration–consolidation model with models of field strength distribution, pore evolution, and the resulting cell damage distribution. Moreover, the effect of electrically induced damage to tissue on extracellular permeability k_e must be evaluated.

3.2. Parametrical study

To study the sensitivity of the model to parameter variations we present a parametrical study for four parameters. Note that the parameters that remain constant as each examined parameter is varied were taken from Table 2 and were estimated for sugarbeet tissue from literature or experiments. This tissue thus represents our model tissue throughout the parametrical study.

First, we varied the viscosity of the liquid medium μ (Fig. 5a) to demonstrate the effect of different temperatures of the material during pressing. If the process is not isothermal, a possibility of heat accumulation and temperature elevation exists. In industry, pressure processing is also often combined with heat processing (in oil extraction for example). The range of viscosities chosen is based on a range of temperatures between 10 and 50 °C, and given for water. If applied to material with markedly different composition of liquid media (e.g. oil), these viscosities should be adapted to the application. We limited the temperature to 50 °C as the model is no longer applicable at higher temperatures, as it does not account for temperature damage to the material. The remaining parameters were the same as determined for sugarbeet, treated according to Protocol A at 300 V pulse amplitude. Model results are also presented for several ratios of compressibility moduli in intact tissue $G_{\varepsilon,e}/G_{\varepsilon,i}$ (Fig. 5b), to demonstrate possible expression kinetics in highly porous tissues containing considerably larger fractions of extracellular space occupied predominantly by air, as in e.g. apple tissue (Harker et al., 2010). We used parameters obtained for sugarbeet in experiments (Protocol A, 300 V) and varied $G_{\varepsilon,e}$. Furthermore, Fig. 5c shows model results for varying k_i, not as a function of electroporation, but as a function of plant species, as membrane permeability seems to vary considerably between various tissues of different plant species. Modelled tissues include pea epicotyl epidermis ($k_i = 10^{-25}$ m^2), ripe apple tissue ($k_i = 5 \cdot 10^{-25}$ m^2), maize leaves midrib mid parenchyma ($k_i = 10^{-23}$ m^2) and soybean hypocotyl elongating epidermis ($k_i = 3 \cdot 10^{-23}$ m^2). All permeability coefficients were recalculated from hydraulic conductivities obtained from (Tomos, 1988), and model results calculated for the intact tissue permeability (no effects of electroporation). Finally, Fig. 5d shows deformation as a function of time for electroporated sugarbeet tissue (Protocol A, 300 V) when varying external pressure P_E. Validating all of these dependencies is out of the scope of this paper, whose purpose is to introduce the basic model by its theoretical formulation and basic proof of concept.

Results in Fig. 5a show the system is stable with regard to the temperature-dependence of viscosity. However, elevated temperatures damage biological tissues, and the model does not capture these effects. Varying the compressibility modulus of extracellular space and thus changing the $G_{\varepsilon,e}/G_{\varepsilon,i}$ ratio has, for fixed $G_{\varepsilon,i}$, f_p, and P_E, a profound effect on the compressibility of the sample during the initial compression stage (Fig. 5b). As the model does not account for the volumetric relationship between the intra- and extracellular phases and $G_{\varepsilon,e}$ in reality varies with time and treatment parameters, the effects as shown in this simulation should be viewed as overestimations. They do however demonstrate possible behaviour of expression kinetics in tissues with different textural properties. In example, apple tissue has large extracellular compartments of air, and is more compressible than sugarbeet or similar, more compact biological materials. Fig. 5c demonstrates the relative unimportance of intrinsic hydraulic permeability of intact cellular membrane (note the scale on the ordinate axis), which depends on the plant species, originating tissue (epidermal, parenchyma, etc.), moisture content at harvesting, and other conditions. We performed these simulations for an intact membrane only, using available permeability data in literature (Tomos, 1988). We chose to exclude electroporation effects since it would be difficult to reliably estimate compressibility coefficients for electroporated tissues cross-species, since they exhibit significant differences in textural properties. Finally, Fig. 5d gives filtration–consolidation kinetics for different constant external pressures.
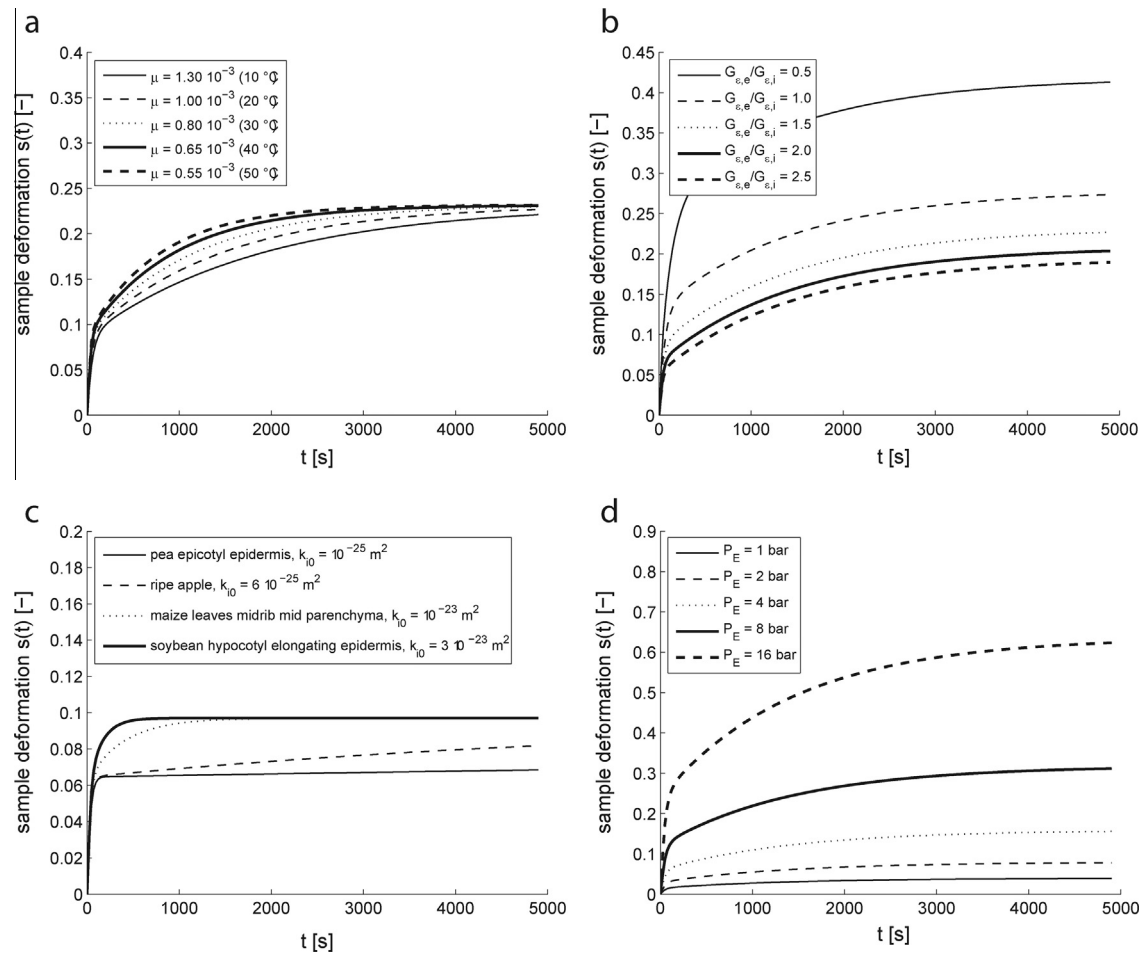
Fig. 5. Results of the parametric model study. (a) Effect of varying the viscosity of the liquid medium μ (temperature variation 10–50 °C); (b) effect of varying the compressibility moduli ratio $G_{\varepsilon,e}/G_{\varepsilon,i}$; (c) effect of varying the intracellular/membrane hydraulic permeability k_i; and (d) effect of variable external pressure P_E.

As anticipated, the resulting profiles are linearly scalable, which is also consistent with various experimental observations, see e.g. experimental results in (Grimi et al., 2010). Since compressibility moduli were determined based on a single pressing experiment at constant external pressure, slight discrepancies between simulated results and experimental data at higher pressures are expected. The compressibility G_ε based on total press-cake deformation is a nonlinear function of pressure for electroporated tissue. See e.g. Fig. 8, pp. 34 in Grimi et al. (2010) for details. Due to this nonlinearity, the compressibility modulus of intracellular space must be recalculated at high pressures.

4. Conclusions

In this work we presented a dual-porosity model for liquid expression from tissue treated by electroporation. The fundamental theory for model construction is rooted in phenomenological observations of liquid flow in porous media.

We connect experiments with the theoretical model through parameter estimation. The experiment-based estimation is necessary at this stage in model development, as biological complexity and diversity render theoretical estimations scarce and unrealistic. We propose means of relating the effects of electroporation on the plasma membrane with membrane hydraulic permeability. This point of model construction invites further development and verification, since theoretical models of electroporation give pore distribution (size, number) as a function of electric field application. There are also an increasing number of experimental studies

available that study pore resealing dynamics and selectivity of the permeabilized plasma membrane. The findings of these studies seem promising for model enhancement, since they describe a temporal dependence of permeability coefficients that we assumed as time-invariable. Inclusion of such dynamics will however most likely require a numerical approach.

In order to keep the model comprehensive in this first account and to focus more on the concept of the dual porosity modelling paradigm in tissue electroporation, we made simplifications with regard to the theory of porous media, which is much more advanced. We intend to elaborate on this issue and develop a more complex model from the consolidation theory point of view in the future. A more complete and complex model is expected to have an added value of reliable predictive capabilities.

We verified the model by fitting simulated consolidation kinetics to experimental data. Based on estimated parameters, we modelled a pressing experiment. The results calculated using optimized initial parameter estimates (compressibility moduli and tissue/membrane permeability) were in good agreement with experimental data; since membrane and tissue permeability are highly variable parameters, we improved our estimates by varying the coefficients within an optimization algorithm. The optimized values were found to be within one order of magnitude from initial estimates, which is acceptable, given the wide range that these parameters normally exhibit, even for a single variety of plant species.

Further work will be dedicated to verification with additional experiments and to extension by combination with a model of

electroporation (pulse protocol effects, pore resealing, etc.). Validation by changing the model material (e.g. apple, carrot, red beet tissue) also poses a potentially interesting challenge.

Appendix A

In this appendix we give a theoretical derivation of factor ξ, which is a constitutive member of the dimensionless parameter α, found in model equations (Eqs. (15) and (16)). Factor ξ relates the intrinsic hydraulic permeability of the cell membrane and the pressure drop across the membrane with the resulting decrease in intracellular porosity (related to liquid pressure via compressibility) and the increase in extracellular porosity due to expression of liquid from the intracellular to the extracellular space.

We begin the derivation by writing Darcy law for transmembrane flow for a single individual cell

$$q_m = \frac{Q_m}{4\pi r^2} = -\frac{k_m}{\mu}\frac{dp}{dr} \tag{A.1}$$

and integrate both sides across the membrane, where the pressure drop $p_i - p_e$ occurs, obtaining

$$Q_m \int_R^{R+l} \frac{dr}{4\pi r^2} = -\frac{k_m}{\mu}\int_{p_e}^{p_i} dp, \tag{A.2}$$

where l is the thickness of the membrane and R the inner cell radius (i.e. the radius of the cell without the membrane). After carrying out the integration and some rearrangement, we have

$$Q_m = \frac{k_m}{\mu}\frac{4\pi R(R+l)}{l}(p_i - p_e). \tag{A.3}$$

The intra-to-extracellular or transmembrane flow of liquid Q_m results in a change in cell porosity ε_c, which is defined as the ratio of liquid phase to total intracellular volume, thus yielding

$$\frac{Q_m}{V} = \frac{d\varepsilon_c}{dt} = \frac{k_i}{\mu}\frac{3(R+l)}{R^2 l}(p_i - p_e). \tag{A.4}$$

Eq. A.4 is not directly comparable with Eqs. (15) and (16), as A.4 gives cell porosity as a function of time only, due to the spatial integration across the domain of a single cell, while in Eqs. (15) and (16) we have both space- and time-dependent liquid pressure of extracellular and intracellular space, or rather of their respective porosities. We must therefore first obtain a volume-normalized equivalent intracellular porosity. In short,

$$\upsilon_{i-e} = \frac{V_m}{V}\frac{d\varepsilon_c}{dt}, \tag{A.5}$$

and therefore

$$\frac{k_i \xi}{\mu}(p_i - p_e) = \frac{k_i}{\mu}\frac{(R+l)^3 - R^3}{R^3}\frac{3(R+l)}{R^2 l}(p_i - p_e)$$
$$= \frac{k_i}{\mu}\frac{9R(R+l)^2 + 3l^2(R+l)}{R^5}(p_i - p_e). \tag{A.6}$$

From A.6 it immediately follows

$$\xi = \frac{9R(R+l)^2 + 3l^2(R+l)}{R^5}, \tag{A.7}$$

simplifying to $\xi = 9/R^2$ for $R \gg l$, which for spherical geometry equals exactly $(A/V)^2$, the square of the surface-to-volume ratio (also termed specific surface). If the membrane thickness l is not insignificant as compared to cell radius R, the more complex form as given by Eq. A.7 should be used to calculate the geometrical factor ξ, however, in biological tissues used in electroporation experiments, this is never the case. A much greater error than neglecting the influence of finite membrane dimensions and using a simplified specific-surface-squared approximation for ξ as proposed, is already introduced several steps earlier with the assumption of spherical cell geometry, since cells in real biological tissues do not exhibit perfectly spherical geometry.

As a final note, a physical interpretation of Eq. (A.5); in the model that we propose, intracellular porosity and thus liquid pressure is modelled as a continuous differentiable function of space (coord. z) and time. In reality, it is discretized by individual biological cells, within which the liquid pressure is constant. The pressure difference exists only across the membrane and is driving the intracellular liquid into the extracellular space, as extracellular liquid pressure is always lower than intracellular (assuming external pressure initially distributes itself equally on the two phases). Thus, in order to maintain the representation of intracellular space porosity continuous on z, the transmembrane flux has to be averaged over the entire intracellular volume, replacing the local effect of variable permeability of the cell membrane with an average permeability of intracellular space. Upon integrating liquid pressure difference in this equivalent media over one layer of cells, and multiplying by $k_i \xi/\mu$, we will obtain effectively the same liquid expression (change in ε) as we would have if we were to calculate the transmembrane flow Q_m.

References

Aguilera, J.M., Chiralt, A., Fito, P., 2003. Food dehydration and product structure. Trends Food Sci. Technol. 14, 432–437.

Amodeo, G., Dorr, R., Vallejo, A., Sutka, M., Parisi, M., 1999. Radial and axial water transport in the sugar beet storage root. J. Exp. Bot. 50, 509–516.

Bazhal, M., Lebovka, N., Vorobiev, E., 2003. Optimisation of pulsed electric field strength for electroplasmolysis of vegetable tissues. Biosyst. Eng. 86, 339–345.

Bazhal, M., Vorobiev, E., 2000. Electrical treatment of apple cossettes for intensifying juice pressing. J. Sci. Food Agric. 80, 1668–1674.

Bazhal, M.I., Lebovka, N.I., Vorobiev, E., 2001. Pulsed electric field treatment of apple tissue during compression for juice extraction. J. Food Eng. 50, 129–139.

Binkley, C., Wiley, R., 1981. Chemical and physical treatment effects on solid–liquid extraction of apple tissue. J. Food Sci. 46, 729–732.

Bouzrara, H., Vorobiev, E., 2003. Solid-liquid expression of cellular materials enhanced by pulsed electric field. Chem. Eng. Process. 42, 249–257.

Buttersack, C., Basler, W., 1991. Hydraulic conductivity of cell-walls in sugar-beet tissue. Plant Sci. 76, 229–237.

De Monte, F., Pontrelli, G., Becker, S., 2013. Drug release in biological tissues. In: Becker, S.M., Kuznetsov, A.V. (Eds.), Transport in Biological Media. Elsevier, Boston, pp. 59–118 (Chapter 3).

Ersus, S., Barrett, D.M., 2010. Determination of membrane integrity in onion tissues treated by pulsed electric fields: use of microscopic images and ion leakage measurements. Innov. Food Sci. Emerg. Technol. 11, 598–603.

Fincan, M., Dejmek, P., 2002. In situ visualization of the effect of a pulsed electric field on plant tissue. J. Food Eng. 55, 223–230.

Grimi, N., Vorobiev, E., Lebovka, N., Vaxelaire, J., 2010. Solid–liquid expression from denaturated plant tissue: filtration–consolidation behaviour. J. Food Eng. 96, 29–36.

Haberl, S., Miklavcic, D., Sersa, G., Frey, W., Rubinsky, B., 2013. Cell membrane electroporation-Part 2: the applications. IEEE Electr. Insul. Mag. 29, 29–37.

Halder, A., Datta, A.K., Spanswick, R.M., 2011. Water transport in cellular tissues during thermal processing. AICHE J. 57, 2574–2588.

Harker, F.R., Redgwell, R.J., Hallett, I.C., Murray, S.H., Carter, G., 2010. Texture of Fresh Fruit. In: Janick, J. (Ed.), Horticultural Reviews. John Wiley & Sons, Inc., pp. 121–224.

Knorr, D., Geulen, M., Grahl, T., Sitzmann, W., 1994. Food application of high-electric-field pulses. Trends Food Sci. Technol. 5, 71–75.

Kotnik, T., Kramar, P., Pucihar, G., Miklavcic, D., Tarek, M., 2012. Cell membrane electroporation- Part 1: The phenomenon. IEEE Electr. Insul. Mag. 28, 14–23.

Krassowska, W., Filev, P.D., 2007. Modeling electroporation in a single cell. Biophys. J 92, 404–417.

Lanoiselle, J.L., Vorobyov, E.I., Bouvier, J.M., Piar, G., 1996. Modeling of solid/liquid expression for cellular materials. AICHE J. 42, 2057–2068.

Lebovka, N.I., Praporscic, I., Vorobiev, E., 2004. Effect of moderate thermal and pulsed electric field treatments on textural properties of carrots, potatoes and apples. Innov. Food Sci. Emerg. Technol. 5, 9–16.

Llano, K.M., Haedo, A.S., Gerschenson, L.N., Rojas, A.M., 2003. Mechanical and biochemical response of kiwifruit tissue to steam blanching. Food Res. Int. 36, 767–775.

Luengo, E., Alvarez, I., Raso, J., 2013. Improving the pressing extraction of polyphenols of orange peel by pulsed electric fields. Innov. Food Sci. Emerg. Technol. 17, 79–84.

Mahnič-Kalamiza, S., Miklavčič, D., Vorobiev, E., 2014. Dual-porosity model of solute diffusion in biological tissue modified by electroporation. Biochim. Biophys. Acta accepted for publication, n/a.

Mhemdi, H., Bals, O., Grimi, N., Vorobiev, E., 2012. Filtration diffusivity and expression behaviour of thermally and electrically pretreated sugar beet tissue and press-cake. Sep. Purif. Technol. 95, 118–125.

Neu, W.K., Neu, J.C., 2009. Theory of Electroporation. In: Efimov, I.R., Kroll, M.W., Tchou, P.J. (Eds.), Cardiac Bioelectric Therapy: Mechanisms and Practical Implications. Springer.

Pavlin, M., Miklavcic, D., 2008. Theoretical and experimental analysis of conductivity, ion diffusion and molecular transport during cell electroporation - Relation between short-lived and long-lived pores. Bioelectrochemistry 74, 38–46.

Pavlin, M., Miklavčič, D., 2008. Theoretical and experimental analysis of conductivity, ion diffusion and molecular transport during cell electroporation — relation between short-lived and long-lived pores. Bioelectrochemistry 74, 38–46.

Petryk, M., Vorobiev, E., 2007. Liquid flowing from porous particles during the pressing of biological materials. Comput. Chem. Eng. 31, 1336–1345.

Petryk, M., Vorobiev, E., 2013. Numerical and analytical modeling of solid–liquid expression from soft plant materials. AIChE J. 59, 4762–4771.

Poel, P.W. van der, Schiweck, H.M., Schwartz, T.K., 1998. Sugar Technology: Beet and Cane Sugar Manufacture. Verlag Dr Albert Bartens KG.

Praporscic, I., Lebovka, N.I., Ghnimi, S., Vorobiev, E., 2006. Ohmically heated, enhanced expression of juice from apple and potato tissues. Biosyst. Eng. 93, 199–204.

Sack, M., Eing, C., Berghoefer, T., Buth, L., Staengle, R., Frey, W., Bluhm, H., 2008. Electroporation-assisted dewatering as an alternative method for drying plants. IEEE Trans. Plasma Sci. 36, 2577–2585.

Saulis, G., 2010. Electroporation of cell membranes: the fundamental effects of pulsed electric fields in food processing. Food Eng. Rev. 2, 52–73.

Saulis, G., Saule, R., 2012. Size of the pores created by an electric pulse: Microsecond vs millisecond pulses. Biochim. Biophys. Acta-Biomembr. 1818, 3032–3039.

Saulis, G., Saulė, R., 2012. Size of the pores created by an electric pulse: microsecond vs millisecond pulses. Biochim. Biophys. Acta 1818, 3032–3039.

Schilling, S., Alber, T., Toepfl, S., Neidhart, S., Knorr, D., Schieber, A., Carle, R., 2007. Effects of pulsed electric field treatment of apple mash on juice yield and quality attributes of apple juices. Innov. Food Sci. Emerg. Technol. 8, 127–134.

Schwartzberg, H.G., 1997. Expression of fluid from biological solids. Sep. Purif. Methods 26, 1–213.

Shankar, D., Agrawal, Y.C., Sarkar, B.C., Singh, B.P.N., 1997. Enzymatic hydrolysis in conjunction with conventional pretreatments to soybean for enhanced oil availability and recovery. J. Am. Oil Chem. Soc. 74, 1543–1547.

Shirato, M., Murase, T., Iwata, M., Nakatsuka, S., 1986. The terzaghi-voigt combined model for constant-pressure consolidation of filter cakes and homogeneous semisolid materials. Chem. Eng. Sci. 41, 3213–3218.

Šuklje, L., 1969. Rheological aspects of soil mechanics. Wiley-Interscience.

Tomos, A.D., 1988. Cellular water relations of plants. In: Franks, F. (Ed.), Water Science Reviews 3, Water Science Reviews. Cambridge University Press.

Vicente, A.R., Costa, M.L., Martínez, G.A., Chaves, A.R., Civello, P.M., 2005. Effect of heat treatments on cell wall degradation and softening in strawberry fruit. Postharvest Biol. Technol. 38, 213–222.

Vorobiev, E., Lebovka, N., 2010. Enhanced extraction from solid foods and biosuspensions by pulsed electrical energy. Food Eng. Rev. 2, 95–108.

Wiktor, A., Witrowa-Rajchert, D., 2012. Applying pulsed electric field to enhance plant tissue dehydration process. ZYWN.-Nauk Technol. Jakosc 19, 22–32.

Zhu, H.X., Melrose, J.R., 2003. A mechanics model for the compression of plant and vegetative tissues. J. Theor. Biol. 221, 89–101.